Supporting Materials

Perovskite $Na_{0.5}Bi_{0.5}TiO_3$: Potential Family of Peculiar Lead-free Electrostrictors

Jie Yin[1], Gang Liu[1], Chunlin Zhao[1], Yanli Huang[1], Jing-Feng Li[2], Zhitao Li[2], Xingmin Zhang[3], Ke Wang[2,b] and Jiagang Wu[1,a]

[1]*Department of Materials Science, Sichuan University, 610064, Chengdu, P. R. China*

[2]*School of Materials Science and Engineering, Tsinghua University, 100084*, *Beijing, P. R. China*

[3]*Shanghai Synchrotron Radiation Facility, Shanghai Institute of Applied Physics, Chinese Academy of Sciences, Pudong New Area, Shanghai 201204, P. R. China*

* Corresponding author:

a) msewujg@scu.edu.cn and wujiagang0208@163.com;

b) wang-ke@tsinghua.edu.cn

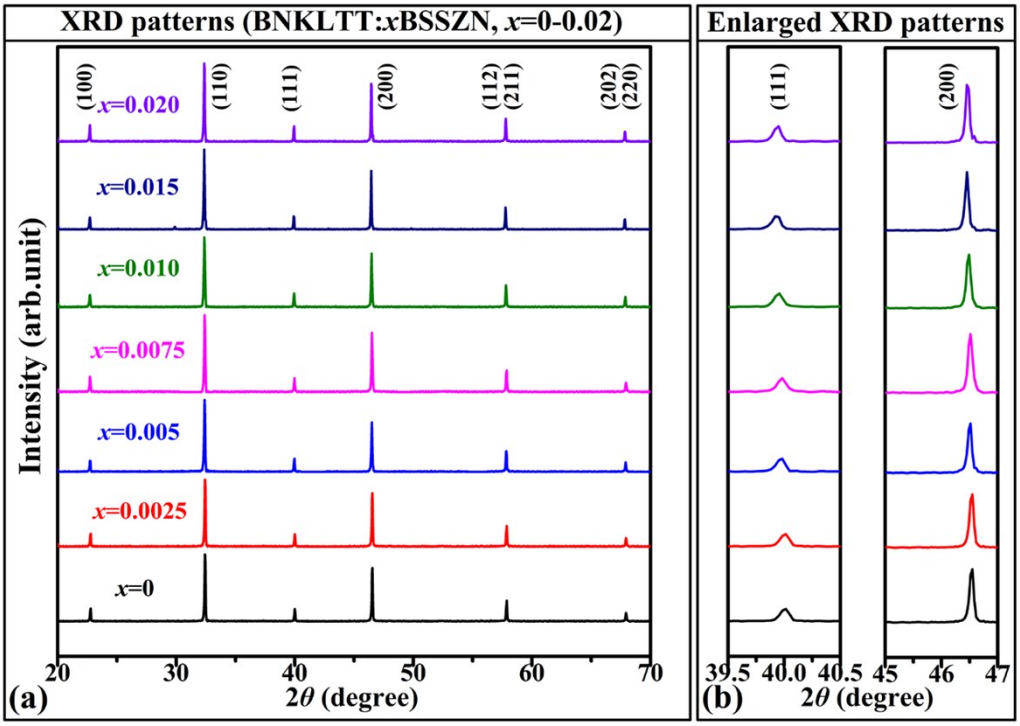

Figure S1. Average phase structure: Normal XRD patterns of unpoled NBKLST-*x*SBSZN samples with different SBSZN compositions (*x*=0, 0.0025, 0.005, 0.0075, 0.010, 0.015, 0.020).

XRD patterns of the unpoled NBKLST-*x*SBSZN samples (*x*=0, 0.0025, 0.005, 0.0075, 0.010, 0.015, 0.020) are shown in Fig. S1. All compositions possess a typical perovskite phase, indicating the formation of the homogeneous solid solution. As can be seen in their expanded XRD patterns, all samples exhibit a pseudocubic structure without any obvious splitting peaks near 40° [indexed by (111)] and 46.5° [indexed by (200)], which belongs to be a characteristic of relaxor ferroelectrics [1].

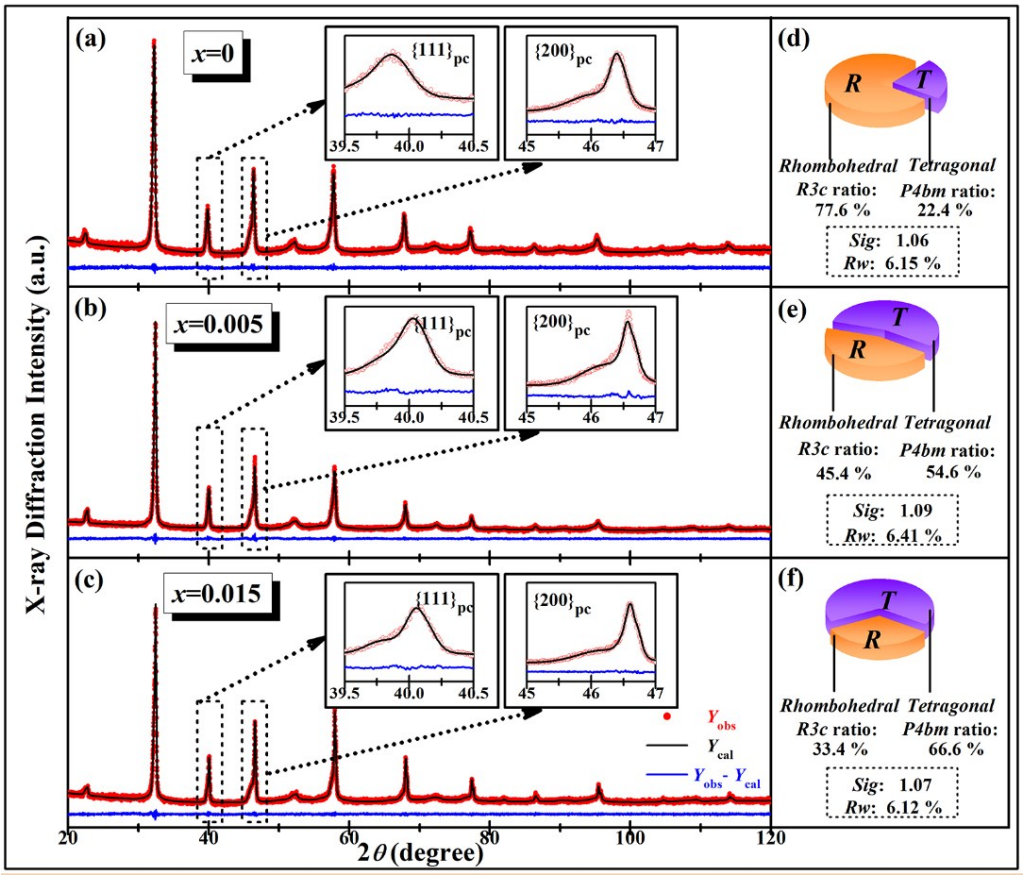

Figure S2: Composition-induced evolutions of the average phase structure. (a-c) Rietveld fitted room temperature XRD plots and (d-f) the corresponding fitted parameters for selected compositions of the A.C.-field poled NBKLST-*x*SBSZN samples.

As shown in Figure S2, *R3c* and *P4bm* are utilized to fit the room temperature XRD plots for selected compositions (x=0, 0.005, 0.015) of the A.C.-field poled NBKLST-*x*SBSZN samples. The corresponding fitted parameters are provided in Table S1 and Figs. S2d-S2f, and the fitted results show that the *P4bm*(T)/*R3c*(R) ratio is rising with the increasing SBSZN compositions.

Table S1 Rietveld refinement results for selected compositions (x=0, 0.005, 0.015) of the A.C.-field poled NBKLST-xSBSZN samples.

	SG	a(Å)	b(Å)	c(Å)	content	sig	Rw
x=0	(R) R3c	5.5014	5.5014	13.5411	0.776	1.06	6.15
	(T) P4bm	5.5473	5.5473	3.9104	0.224		
x=0.005	(R) R3c	5.5344	5.5344	13.4183	0.454	1.09	6.41
	(T) P4bm	5.5742	5.5742	3.9143	0.546		
x=0.015	(R) R3c	5.5090	5.5090	13.6694	0.334	1.07	6.12
	(T) P4bm	5.6672	5.6672	3.9511	0.666		

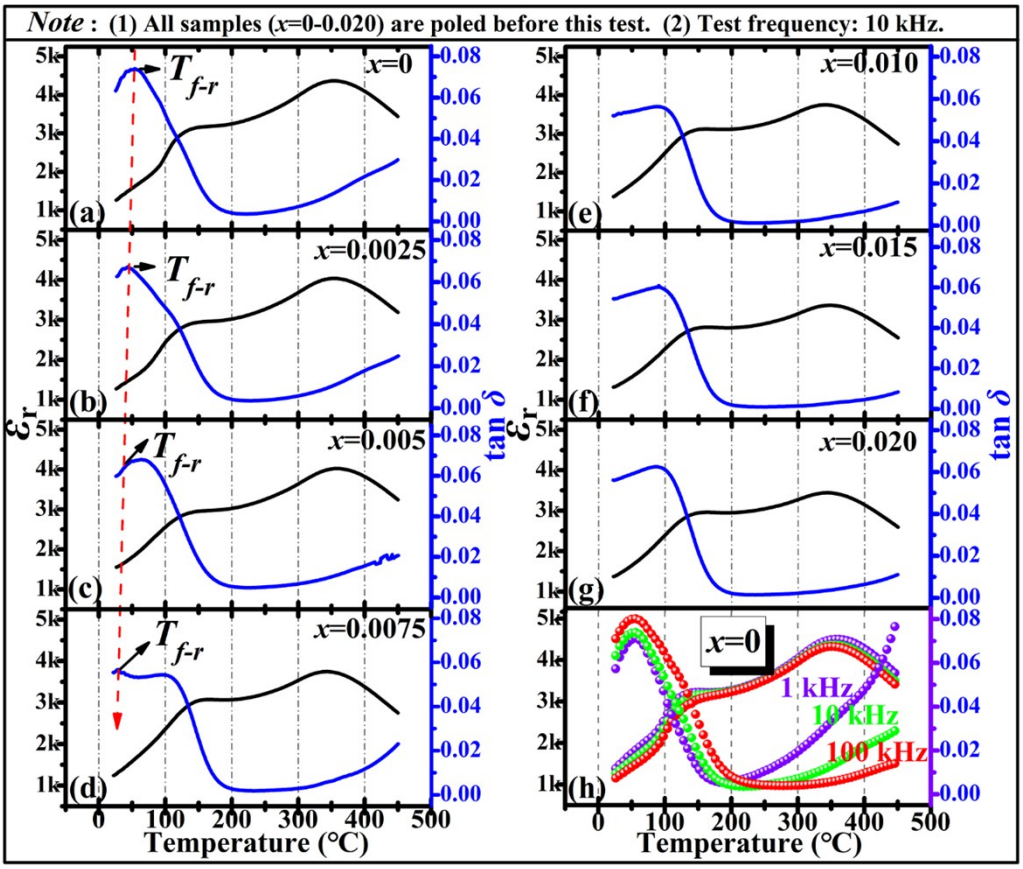

Figure S3: Dielectric information: (a-g) Temperature-dependent relative dielectric constant (ε_r) and loss tangent (tan δ) of NBKLST-xSBSZN (x=0, 0.0025, 0.005, 0.0075,

0.010, 0.015, 0.020) samples measured at 10 kHz. The black arrows give the $T_{f\text{-}r}$ detected from the tan δ-T curves, while the red arrows show the variation tendency of $T_{f\text{-}r}$ with the increasing SBSZN compositions. (h) Temperature-dependent relative dielectric constant (ε_r) and loss tangent (tan δ) of the NBKLST (x=0) composition measured at 1 kHz, 10 kHz and 100 kHz.

Figures S3a-S3g show the temperature dependence of dielectric permittivity (ε_r) and dielectric loss (tan δ) of NBKLST-xSBSZN samples as a function of x, measured at 10 kHz. It is previously reported that three dielectric anomalies can be observed in BNT-based ceramics system, including the ferroelectric to relaxor transition temperature $T_{f\text{-}r}$ (or closely depolarization temperature T_d), the first dielectric maximum T_{fm}, and the second dielectric maximum T_{sm} [2]. The black arrows give the $T_{f\text{-}r}$ detected from the tan δ-T curves, while the red arrows show the variation tendency of $T_{f\text{-}r}$ with the increasing SBSZN compositions. From Fig. S3h, one can see that the dielectric (ε_r-T and tan δ-T) curves of the NBKLST sample exhibit two diffused and frequency dispersive peaks. As the frequency increases, their ε_r values will get decreased and their maximums are slightly shifted towards higher temperatures. In addition, their ε_r values show a pronounced dependence on the frequencies when $T \leq 200$ ℃. All these characteristics further demonstrate the relaxor nature of NBT-based samples in this work [1].

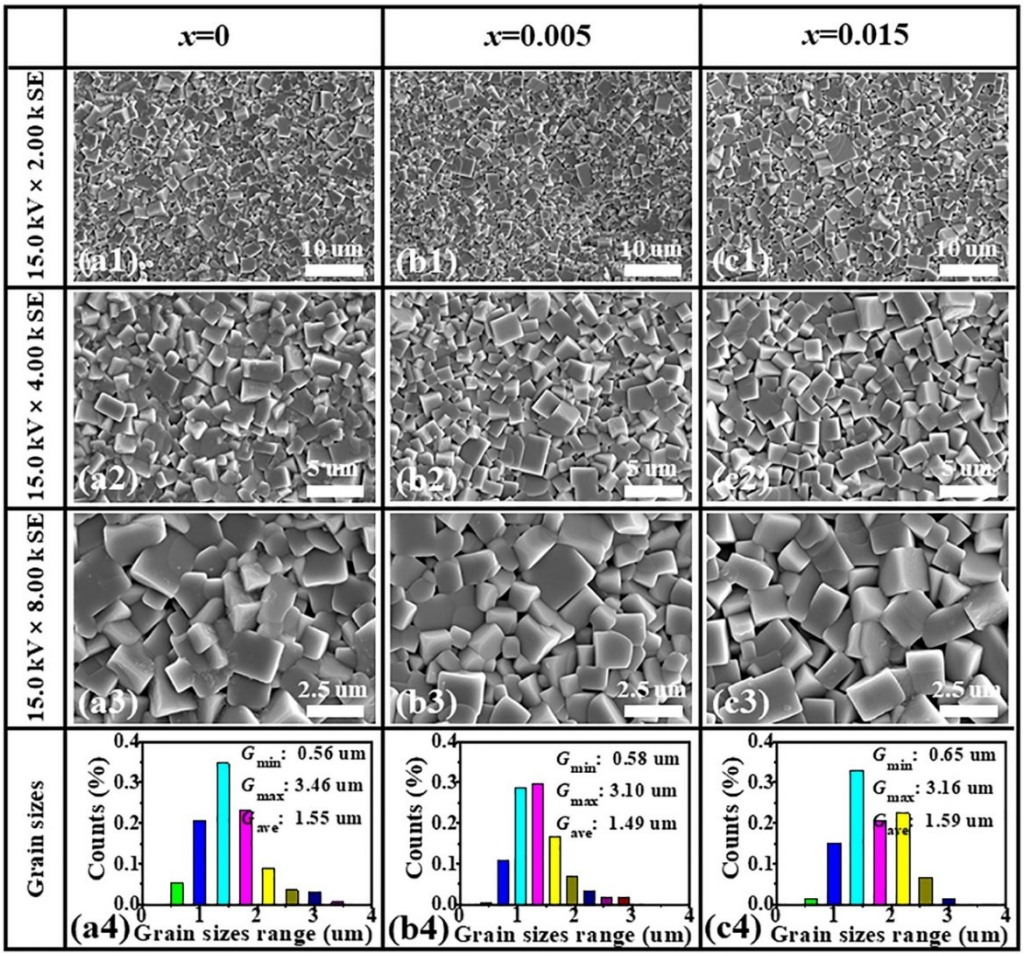

Figure S4. Microstructure part: Grain morphology and grain sizes distribution of the selected compositions (x=0, 0.005, 0.015).

FE-SEM images and corresponding grain sizes distribution analysis of selected compositions (x=0, 0.005, 0.015) are given in Fig. S4. Grains of all samples exhibit the neat rectangular shapes with clear grain boundaries, and grain sizes of these samples exhibit no obviously dependence on the composition. Therefore, the intrinsic structural evolution should contribute to the variations of electrical properties rather than the effects of the grain sizes, as discussed in our main text.

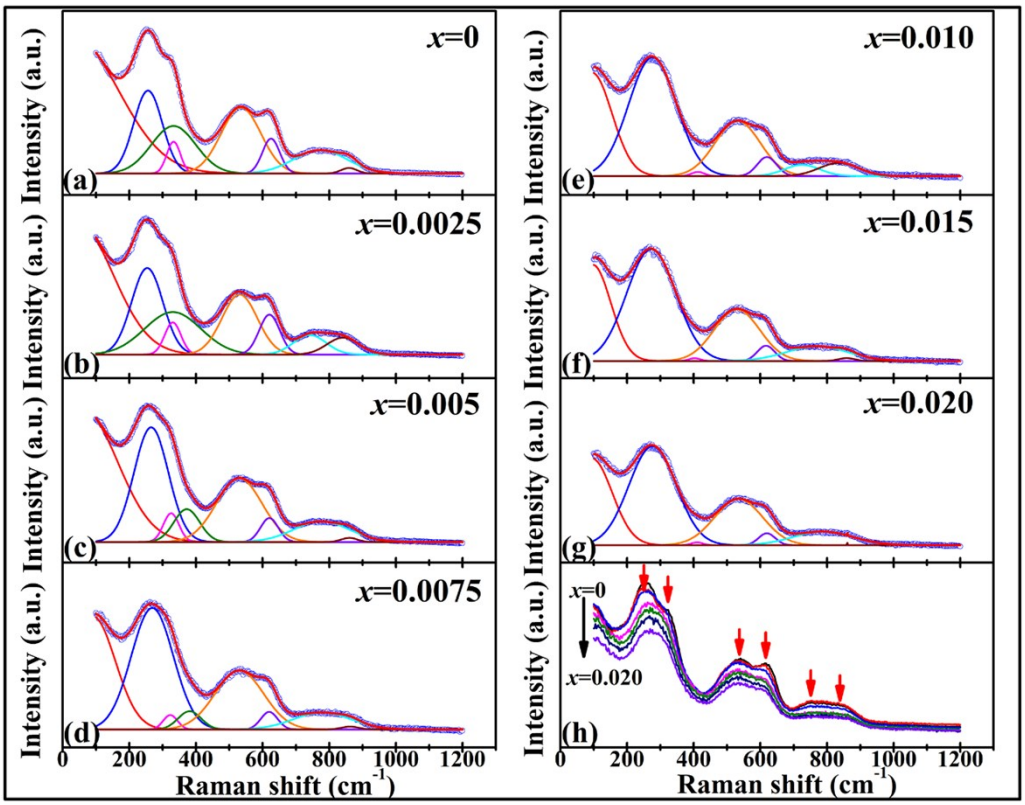

Figure S5. (a-g) Composition-dependent Raman spectroscopy for NBKLST-*x*SBSZN (*x*=0, 0.0025, 0.005, 0.0075, 0.010, 0.015, 0.020) samples in the range from 100 to 1200 cm^{-1}. The spectra are deconvoluted according to 8 Lorentzian peak functions. (f) The merged Raman curves of different compositions to better illustrate the composition-induced evolution of Raman spectra.

Raman spectra of the poled samples are deconvoluted into eight Lorentzian-shaped peaks, as shown in Figs. S5a-S5g, respectively. According to the eight fitted Lorentzian peaks, wavenumber, intensity and FWHM (full width at half maximum) data of six representative modes (*A*, *B1-B3*, *C2-C4*) are derived, as shown in our main text. The merged Raman curves are utilized to better illustrate the composition-induced evolution of typical Raman vibration modes, as the red arrows marked in Fig. S5h.

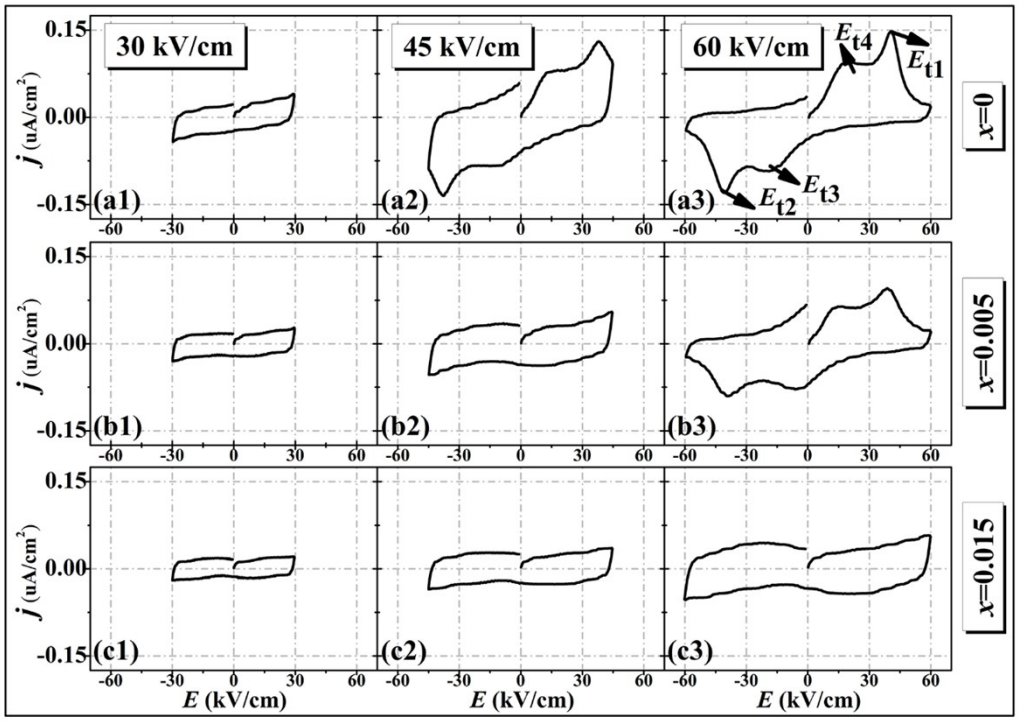

Figure S6. Current-electric field (*j*-*E*) loops of the selected NBKLST-*x*SBSZN compositions (*x*=0, 0.005, 0.015) under different electric field (*E*=30 kV/cm, 45 kV/cm and 60 kV/cm). The black arrows shown in Fig. S6a3 represent the transition between the RE and FE state, where E_{t1}/ E_{t2} arrows represent the RE to FE transition and E_{t3}/ E_{t4} arrows represent the FE to RE transition.

Figure S6 provides the current density versus electric field (*j*-*E*) curves of the selected NBKLST-*x*SBSZN compositions (*x*=0, 0.005, 0.015), measured under different electric field (*E*=30 kV/cm, 45 kV/cm and 60 kV/cm). E_{t1}/ E_{t2} arrows marked on the peaks of *j*-*E* loops represent the RE to FE transition, and these data are utilized to depict the profile of the RE to FE transition shown in Fig. 5d in our main text.

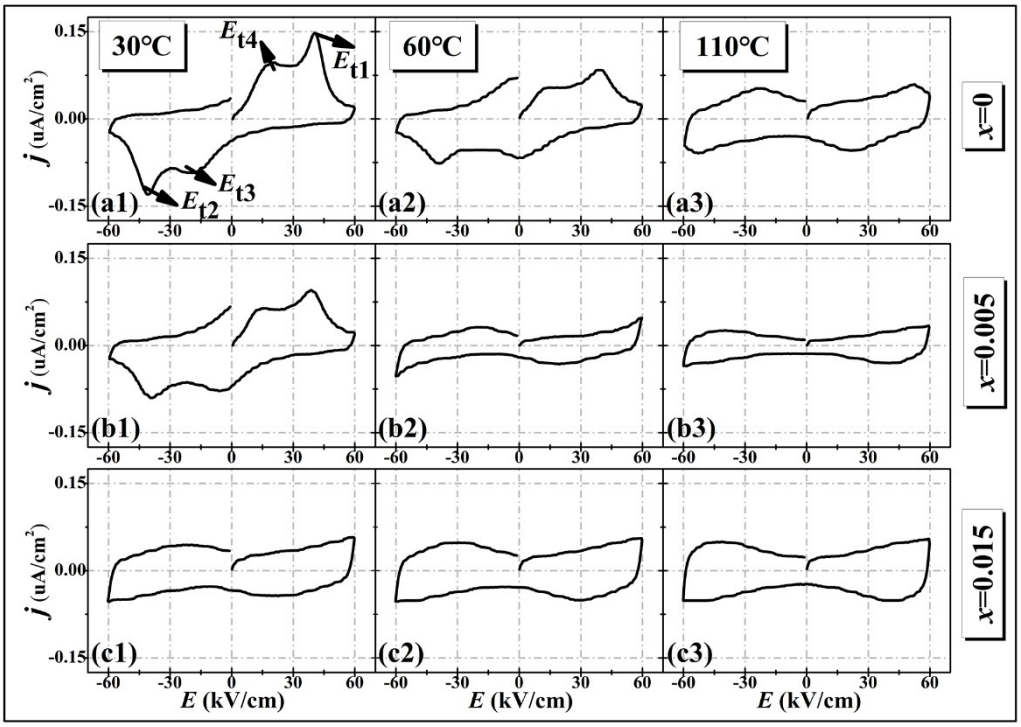

Figure S7. Current-electric field (*j*-*E*) loops of the selected NBKLST-*x*SBSZN compositions (*x*=0, 0.005, 0.015) under different operating temperatures (*T*=30 ℃, 60 ℃ and 110 ℃). The black arrows shown in Fig. S7a1 represent the transition between the RE and FE state, where E_{t1}/ E_{t2} arrows represent the RE to FE transition and E_{t3}/ E_{t4} arrows represent the FE to RE transition.

Figure S7 provides the current density versus electric field (*j*-*E*) curves of the selected NBKLST-*x*SBSZN compositions (*x*=0, 0.005, 0.015), measured under different operating temperatures (*T*=30 ℃, 60 ℃ and 110 ℃). E_{t1}/ E_{t2} arrows marked on the peaks of *j*-*E* loops represent the RE to FE transition, and these data are utilized to depict the profile of the RE to FE transition shown in Fig. 5d in our main text.

References

[1] Groszewicz, P. B.; Breitzke, H.; Dittmer, R.; Sapper, E.; Jo, W.; Buntkowsky, G.; Rödel, J. Nanoscale phase quantification in lead-free $(Bi_{1/2}Na_{1/2})TiO_3$−$BaTiO_3$ relaxor ferroelectrics by means of Na 23 NMR. *Phys. Rev. B* **2014**, *90*, 220104.

[2] Xu, Q.; Xie, J.; He, Z.; Zhang, L.; Cao, M.; Huang, X.; Liu, H. Energy-storage properties of $Bi_{0.5}Na_{0.5}TiO_3$-$BaTiO_3$-$KNbO_3$ ceramics fabricated by wet-chemical method. *J. Eur. Ceram. Soc.* **2017**, *37*, 99.